Original Article

JCBFM

Journal of Cerebral Blood Flow & Metabolism
2019, Vol. 39(1) 44–57

DOI: 10.1177/0271678X17736963
journals.sagepub.com/home/jcbfm
SAGE

A mouse model of subcortical vascular dementia reflecting degeneration of cerebral white matter and microcirculation

Eek-Sung Lee[1,2,3], Jin-Hui Yoon[2,4], Jiye Choi[2,4], Faris R Andika[4], Taekwan Lee[5] and Yong Jeong[2,4]

Abstract

Subcortical vascular dementia (SVaD) is associated with white matter damage, lacunar infarction, and degeneration of cerebral microcirculation. Currently available mouse models can mimic only partial aspects of human SVaD features. Here, we combined bilateral common carotid artery stenosis (BCAS) with a hyperlipidaemia model in order to develop a mouse model of SVaD; 10- to 12-week-old apolipoprotein E (ApoE)-deficient or wild-type C57BL/6J mice were subjected to sham operation or chronic cerebral hypoperfusion with BCAS using micro-coils. Behavioural performance (locomotion, spatial working memory, and recognition memory), histopathological findings (white matter damage, microinfarctions, astrogliosis), and cerebral microcirculation (microvascular density and blood–brain barrier (BBB) integrity) were investigated. ApoE-deficient mice subjected to BCAS showed impaired locomotion, spatial working memory, and recognition memory. They also showed white matter damage, multiple microinfarctions, astrogliosis, reduction in microvascular density, and BBB breakdown. The combination of chronic cerebral hypoperfusion and ApoE deficiency induced cognitive decline and cerebrovascular pathology, including white matter damage, multiple microinfarctions, and degeneration of cerebral microcirculation. Together, these features are all compatible with those of patients with SVaD. Thus, the proposed animal model is plausible for investigating SVaD pathophysiology and for application in preclinical drug studies.

Keywords

Atherosclerosis, blood–brain barrier, cerebral blood flow, microcirculation, vascular cognitive impairment

Received 14 November 2016; Revised 12 September 2017; Accepted 13 September 2017

Introduction

Vascular dementia, a heterogeneous clinical entity in which cognitive impairment is attributed to any number of vascular pathologies, is the second most common cause of dementia after Alzheimer's disease (AD). Vascular dementia is more prevalent in East Asian countries than in Western countries.[1] Due to an aging population, an increase in cerebrovascular disease has led to projections of a surge in the prevalence of vascular dementia over the next three decades.[2] In spite of the growing importance of therapeutic intervention for vascular dementia, preclinical drug studies have been hampered by a lack of adequate experimental models.

Subcortical vascular dementia (SVaD) is the most common subtype of vascular dementia and exhibits

[1]Graduate School of Medical Science and Engineering, Korea Advanced Institute of Science and Technology (KAIST), Daejeon, Republic of Korea
[2]KI for Health Science and Technology, Korea Advanced Institute of Science and Technology (KAIST), Daejeon, Republic of Korea
[3]Department of Neurology, Soonchunhyang University Bucheon Hospital, Gyeonggi-do, Republic of Korea
[4]Department of Bio and Brain Engineering, Korea Advanced Institute of Science and Technology (KAIST), Daejeon, Republic of Korea
[5]Laboratory Animal Center, Daegu-Gyeongbuk Medical Innovation Foundation (DGMIF), Daegu, Republic of Korea

The first two authors contributed equally to this work.

Corresponding author:
Yong Jeong, Department of Bio and Brain Engineering, Korea Advanced Institute of Science and Technology (KAIST), 291 Daehak-ro, Yuseong-gu, Daejeon 34141, Republic of Korea.
Email: yong@kaist.ac.kr

relatively uniform clinical and pathological features.[3,4] Pathologic hallmarks of SVaD include white matter lesions (leukoaraiosis) and multiple small discrete infarctions (lacunar infarctions).[4–6] These pathologic changes may be manifested even in the early stages of SVaD, and contribute to neurological deficits and neurobehavioral symptoms such as gait disturbance, apathy, abulia, aspontaneity, agitation, disinhibition, frontal executive dysfunctions, and memory impairment due to inadequate retrieval strategies.[7] Other pathological features associated with SVaD include alterations of cerebral microcirculations, such as accumulations of erythrocyte, basement membrane thickening, pericyte degeneration, and blood–brain barrier (BBB) breakdown.[8–10] Studies of BBB breakdown in patients with SVaD have revealed increased permeability not only in white matter lesions but also in normal white matter.[11–14] These findings suggest that alterations of cerebral microcirculations precede white matter lesions and contribute to the pathologic progress.

Most animal research on dementia have focused almost exclusively on mouse models of AD, whereas only limited research has been performed on other forms of dementia including SVaD. A mouse model of chronic cerebral hypoperfusion generated by bilateral common carotid artery stenosis (BCAS) surgery provides good reproducibility of the white matter lesions and behavioural deficit relevant to human SVaD.[15,16] However, shortcomings of the BCAS include the fact that researchers must wait over six months after BCAS surgery to obtain apparent pathological and behavioural features.[17] In addition, the BCAS model does not induce multiple microinfarctions or alterations in cerebral microcirculations.

Apolipoprotein E (ApoE) is responsible for the transport of cholesterol and other lipids, as well as for mediating the clearance of plasma lipoproteins.[18] The ApoE knock-out ($^{-/-}$) mouse, a classic and widely used model of atherosclerosis, begins to develop severe hypercholesterolemia and atherosclerotic lesions in the aorta and pulmonary, coronary, and carotid arteries at the age of 8 to 10 weeks.[19] In addition to its well-defined role in atherosclerosis, ApoE plays a central role in cerebral microcirculation maintenance. One notable study demonstrated that BBB breakdown and microvascular degeneration is caused by a direct loss of the inhibitory effect of ApoE on the activation of the cyclophilin A-nuclear factor-kB-matrix metalloproteinase-9 pathway.[20]

Taking advantage of the BCAS model, which can be applicable to transgenic or knockout mice, we established a mouse model of SVaD using ApoE$^{-/-}$ mice. Our mouse model might herald important improvements in preclinical, pharmacological SVaD research.

Materials and methods

Experimental animals and surgery

All experimental procedures were approved by the Korea Advanced Institute of Science and Technology Institutional Animal Care and Use Committee (KA2013-53). Animal care and handling were carried out according to Korea Advanced Institute of Science and Technology Institutional Animal Care and Use Committee guidelines. Experiments are performed and reported in accordance with the ARRIVE (Animal Research: Reporting in vivo Experiments) guidelines (https://www.nc3rs.org.uk/arrive-guidelines). Wild-type (C57BL/6J) mice were purchased from the Korea Research Institute of Bioscience and Biotechnology (KRIBB) and maintained in a pathogen-free animal facility at KAIST. ApoE$^{-/-}$ (backcrossed onto the C57BL/6J background for more than 10 generations) mice were kindly donated to us from the colony of Professor CH Lee at the Laboratory Animal Resource Centre, KRIBB, University of Science and Technology, and maintained in a pathogen-free animal facility at KAIST. When the ApoE$^{-/-}$ mice were four weeks old, they were started on a high-fat diet for up to 10 weeks. During this time, 44.8% of the total caloric intake of these mice was derived from fat (TD.06415, Harlan Teklad). Food and water were available ad libitum.

To induce chronic cerebral hypoperfusion, male wild-type or ApoE$^{-/-}$ mice were subjected to either sham or BCAS operations using micro-coils, as previously described.[16] Briefly, mice were anesthetized with isoflurane via a facial mask and placed in a dorsal recumbent position on a heated blanket (Harvard Homoeothermic Blanket Control Unit, Harvard Apparatus, MA, USA); rectal temperature was maintained at 37.0°C. A midline skin incision was made, and the underlying fat tissue was retracted using a self-retaining retractor (Colibri retractor, Fine Science Tolls, North Vancouver, Canada). Both common carotid arteries (CCA) were exposed and dissected from carotid sheaths; arteries were lifted by two 6–0 black silk sutures. Micro-coils (Sawane Spring Co., Shizuoka, Japan), with an internal diameter of 0.18 mm, were implanted by rotating them around both CCAs. Sham-operated mice underwent identical surgical procedure without inserting the micro-coils. The incision was closed with a black silk suture, and mice were returned to an animal holding area immediately after surgery.

Study design

Male mice, aged 10 to 12 weeks, were divided into four groups based on genotype and operative procedure: (1) wild-type, sham-operated; (2) wild-type, BCAS-operated; (3) ApoE$^{-/-}$, sham-operated; and (4) ApoE$^{-/-}$,

BCAS-operated. Temporal changes in cerebral blood flow (CBF) were measured before and one, three, and seven days after surgery, while behavioural experiments were performed four weeks after sham- or BCAS operations. Six weeks after surgery, in vivo multi-photon imaging, magnetic resonance imaging (MRI) and histopathological examinations were performed. ApoE$^{-/-}$ and wild-type mice were randomly assigned to the BCAS or sham-operation groups. Mice were randomly assigned via random number generation. All surgeries performed by an investigator (E.-S.L.) blinded to the genotype of each animal. The investigators responsible for histological analysis (J.-H.Y. and F.R.A), MRI (T.-K.L), and behavioural experiments (J.C.) were blinded and unaware of group allocation throughout the experiments.

Cerebral blood flow measurements via laser-Doppler flowmetry

CBF in the right parietal cortex was measured in all groups (six mice per group). Under isoflurane anaesthesia, a custom-made guide cannula for laser-Doppler flowmetry (LDF) was secured onto the skull, 1.0 mm posterior to bregma and 2.5 mm lateral to the midline, using dental cement. The guide cannula was constructed with a 3D printer using photopolymer. CBF was recorded by placing a 26-gauge LDF probe (BLF21, Transonic Systems Inc., Ithaca, NY, USA) through the guide cannula. CBF was measured immediately before surgeries to obtain baseline values, and 2 h, one, three, and seven days after surgery. For each measurement, signals obtained over the course of 5 min were averaged. Rectal temperature was maintained at 37°C during all measurements.

Magnetic resonance imaging

T2-weighted imaging and magnetic resonance angiography (MRA) were conducted using a Bruker 9.4-T preclinical MRI at DGMIF. Briefly, wild-type and ApoE$^{-/-}$ mice that had undergone BCAS or a sham operation were anesthetized with isoflurane, placed on an MRI cradle, and inserted into the MRI scanner. Thirty-one consecutive coronal T2-weighted images were acquired (256×128, field of view of 3×3 cm, repetition time/echo time = 3000/60 ms, and two averages). For the MRA, a time-of-flight angiogram was acquired using a three-dimensional (3D) gradient echo sequence with an echo time of 2.8 ms and a repetition time of 18 ms. The field of view was $20 \times 20 \times 20$ mm, spatial resolution was $78 \times 78 \times 156$ μm, and total scan time was about 8 min. The maximum intensity projection revealed arterial vessel projections of the mouse head and brain.

Histopathological examination

Six weeks after surgery, BCAS- or sham-operated mice were deeply anesthetized by intraperitoneal injection of ketamine (100 mg/kg) and xylazine (10 mg/kg), and perfused transcardially with phosphate-buffered saline (PBS), followed by 4% paraformaldehyde. For immunofluorescence staining, brains were transferred to 30% (w/v) sucrose for 48 h after overnight post-fixation. Cryoprotected brains were embedded using optimal cutting temperature compound, and frozen in dry ice-cooled isopentane. Coronal brain sections 30 μm in thickness were produced, collected, washed, and blocked in 5% normal donkey serum in PBS and 0.01% Triton X-100. Free-floating sections were then incubated in primary antibodies overnight at 4°C, followed by incubation in fluorophore-conjugated secondary antibodies. Details of the primary and secondary antibodies used are provided in Supplementary Table 1. Paraffin blocks were prepared for staining with Luxol Fast Blue (LFB), haematoxylin and eosin (H&E), and immunohistochemistry (IHC) for CD68. LFB, H&E staining, and IHC for CD68 were performed as described previously.[17] The perfused brains were post-fixed in 4% paraformaldehyde at 4°C overnight and dehydrated through a series of graded alcohol solutions using an automatic tissue processor (TP1020, Leica Biosystems, Newcastle, UK). The dehydrated brain tissues were embedded in paraffin blocks and sliced into 4-μm-thick coronal sections using a microtome (RM2245, Leica Microsystems, Germany). The severity of the white matter damage revealed by LFB staining was graded as normal (grade 0), disarrangement of the nerve fibres (grade 1), formation of marked vacuoles (grade 2), and disappearance of myelinated fibres (grade 3) as described previously.[21,22] H&E staining and IHC for CD68 were used to detect any histological changes, including hippocampal neuronal loss and infarctions.[16,17]

All fluorescence-stained brain sections were scanned using an automated microscope (ImageXpress Micro™, Molecular Device) with a 10 × objective lens. Images were processed by MetaXpress software (Molecular Device) and stitched together to generate an entire brain section. The fluorescence intensity was measured on two brain sections per mouse and two areas per section (i.e. four regions of interest per mouse) using ImageJ software. The values measured in the four regions were averaged and used as representative values for each mouse. Brain sections used for LFB, H&E, and IHC staining were scanned using a whole slide imaging system (Axio Scan.Z1; Zeiss; Jena, Germany) with a 20 × objective lens.

In vivo multi-photon imaging

Cranial window preparation. Open-skull cranial windows for in vivo imaging were made as previously

described.[23] Briefly, a craniotomy (2.0 mm × 2.0 mm) was made using a high-speed dental drill over the somatosensory cortex. A custom-made head frame was attached to the skull with dental cement, and the dura was carefully removed with fine forceps. Cerebral blood vessels were imaged using a multi-photon microscope (LSM 510, Zeiss, Oberkochen, Germany) coupled to a femtosecond-pulsed tunable Ti:Sapphire laser (Chameleon Ultra™, Coherent, Inc., Santa Clara, CA, USA) with a water immersion objective lens (20×/1.0 M27, Zeiss).

Perfused capillary length measurement. Fluorescein isothiocyanate (FITC)-conjugated dextran (2 MDa, Invitrogen, 0.2 ml of 10 mg/ml) was injected via the tail vein, and multi-photon images were acquired from 50 μm below the cortical surface up to a depth of 250 μm, with 1.5 μm intervals between each image. A total of 133 Z-stack images were maximally projected and reconstructed using ImageJ software. Perfused capillary (<6 μm in diameter) length, expressed in mm of vessel per mm^3 of brain volume, was determined using the ImageJ plug-in NeuroJ toolbox by a blinded investigator.[24]

Behavioural experiments

Open field test. Locomotor activity was measured using the open field test. The open-field box was made of white plastic (40 × 40 × 40 cm) and divided into a central field (centre, 20 × 20 cm) and an outer field (periphery). Individual mice were placed in the periphery of the field and the paths of the animals were recorded with a video camera. The total distance travelled for 30 min and the time spent in each field were analysed using EthoVision XT (Noldus; Wageningen, Netherlands).

Y-maze test. Spatial working memory was assessed by spontaneous alternation behaviours in the Y-maze test, which was performed as previously described.[25] The maze consisted of three white plastic arms (40 cm long, 10 cm high, and 8.5 cm wide) diverging at a 120° angle from the central point. After each mouse was tested, the floor of the maze was cleaned with 10% ethanol to avoid olfactory cues. Each mouse was placed at the end of the start arm and allowed to move freely through the maze during an 8-min session. Their movement was recorded with a video camera and the number of arm entries was counted manually. An arm entry was considered to be complete when the hind paws of the mouse were completely within the arm. The percentage of spontaneous alternations was calculated as the ratio of actual alternations (entries into all three arms on consecutive occasions) to total alternations (defined as the total number of arm entries minus 2) × 100.

Novel object recognition test. For habituation, a mouse was placed in the empty open-field box (40 × 40 × 40 cm) and allowed to freely explore the open field for 15 min. During the familiarization session, two identical objects were placed in the box and the mouse was allowed to explore them for 10 min. The mouse was considered to "explore" an object when its head was facing within 1 inch of the object. The mouse was then removed from the box. After a 1-h retention interval, the mouse was placed back in the box with two objects in the same locations; one of the familiar objects was replaced by a novel object, and the mouse was then allowed to explore the two objects for 5 min.

Statistical analysis

Statistical analysis was performed using Graph Pad Prism (GraphPad Software, CA, USA). To investigate the effects of genotype and operation, we designed all experiments with 2 × 2 factorial experimental designs with four groups (wild-type sham, wild-type BCAS, $ApoE^{-/-}$-sham, and $ApoE^{-/-}$-BCAS). Two-way analyses of variance (ANOVA) with post hoc analyses were performed for outcome measures except severity score of white matter damage from LFB staining. Severity scale for white matter damage of each group was compared using Chi-square methods. P values less than 0.05 were considered significant, and significance level is indicated using the following asterisk code ($*P < 0.05$, $**P < 0.01$, $***P < 0.001$). Detailed results for the two-way ANOVAs are shown in Supplementary Table 2. A post hoc power analysis was performed using PASS version 12 (PASS 12; NCSS, LLC; Kaysville, Utah, USA; www.ncss.com). The effect size indices were calculated using F-values obtained from ANOVAs with the following assumptions: α 0.05 and standard deviation 20% of mean for variables from each experiment. Statistical power (1−β) was then determined.[26] Detailed results of the power analysis are provided in Supplementary Table 3.

Results

Reduction in cerebral blood flow after BCAS

CBF values of sham- and BCAS-operated wild-type and $ApoE^{-/-}$ mice are provided in Figure 1(a). In the sham-operated mice (wild-type and $ApoE^{-/-}$ groups), CBF values varied from 96.4% to 103.9%respectively, without any significant difference between any time intervals. In the wild-type BCAS group, CBF values significantly decreased 2 h after BCAS (47.9%) from preoperative baseline measures, and began to recover at one day (57.5%) post-operation, reaching up to 75.4% at seven days. In contrast, CBF values in the

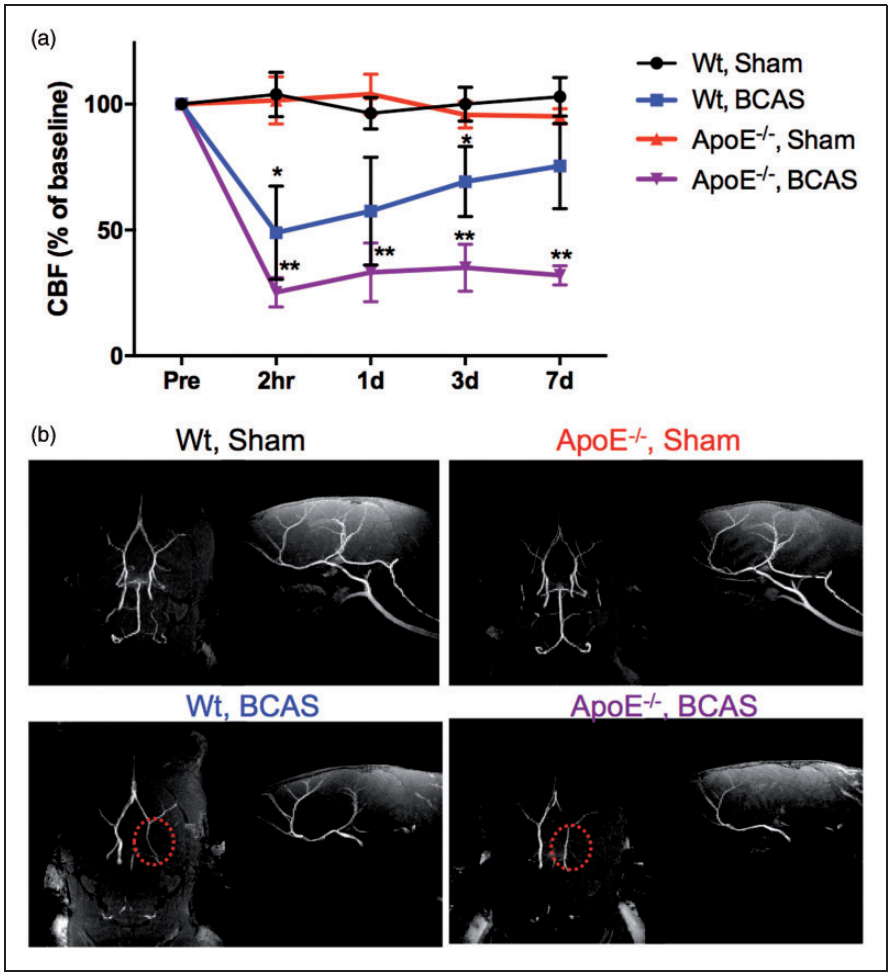

Figure 1. Temporal changes in cortical CBF values. (a) CBF was measured in wild-type sham ($n = 6$), wild-type BCAS ($n = 6$), ApoE$^{-/-}$ sham ($n = 6$), and ApoE$^{-/-}$ BCAS ($n = 6$) mice. CBF values are expressed as a percentage of the baseline CBF values. Mean ± s.e.m. Significance for multiple comparisons: *$P < 0.05$; **$P < 0.01$. (b) Representative MRI angiograms of a mouse brain. (left image: bottom view of the brain; right image: sagittal view of the brain). The circle of Willis was clearly observed in wild-type sham and ApoE$^{-/-}$ sham-operated mice, but not in wild-type BCAS and ApoE$^{-/-}$ BCAS-operated mice (indicated by the red dotted circle in the image). Note that the absence of carotid arteries in the BCAS groups was due to artefacts from the metal micro-coil used for the procedure.

ApoE$^{-/-}$-BCAS group sharply dropped to 25.3% 2 h after BCAS, and continued to decreased one (33.1%), three (35.2%), and seven (32.2%) days after surgery. The level of CBF in the ApoE$^{-/-}$-BCAS group at 1 h, one, three, and seven days after surgery was significantly lower than that of mice in the wild-type sham group. However, CBF levels in the wild-type BCAS group only showed significant differences at 2 h and three days after operation. MRI angiograms of the mouse brain, clearly revealed the circle of Willis in wild-type sham and ApoE$^{-/-}$-sham mice; however, the circle of Willis was less visible for wild-type BCAS and ApoE$^{-/-}$-BCAS mice (Figure 1(b)). Bilateral carotid arteries did not appear in any of the BCAS groups, regardless of genotype, because the metal micro coil used for the BCAS procedure created artefacts in the MRI. When the carotid arteries are occluded, the visual pathway may be injured following the occlusion of the ophthalmic arteries. This may compromise behavioural assessments. The patency of the common carotid artery after the BCAS operation was evaluated before euthanasia using LDF and fluorescence images obtained after intravenous injection of FITC-dextran. The bilateral common carotid arteries were not occluded after the BCAS operation in any of the animals used in the CBF analysis (data not shown).

White matter damage, multiple microinfarctions, and extensive astrogliosis

To investigate whether our mouse model reflected the pathological features of human SVaD, we assessed the

presence of white matter damage, multiple microinfarctions, and astrogliosis using immunofluorescence staining methods.

Wild-type and ApoE$^{-/-}$ mice subjected to chronic cerebral hypoperfusion developed white matter injury. Figure 2(a) shows representative images of immunofluorescent staining for myelin basic protein (MBP). Quantitative analysis of images from the immunostained brain sections indicated that myelin density was decreased by 44.7% and 62.8% in wild-type-BCAS and ApoE$^{-/-}$-BCAS mice, respectively, when compared to sham-operated wild-type mice (Figure 2(b)). A two-way ANOVA followed by Tukey's multiple comparison test revealed significant effects for BCAS operation ($F(1,38) = 40.15$, $P < 0.0001$) and genotype ($F(1,38) = 5.599$, $P = 0.0089$), and no significant interaction between genotype and BCAS operation ($F(1,38) = 0.02038$, $P < 0.8872$). Figure 2(c) shows representative images of LFB staining. Grading scores of LFB staining showed similar tendency, however without statistical significance ($P = 0.13$) probably due to the small sample size for categorical grading (Figure 2(d)). T2-weighted MRI revealed no apparent white matter hyperintensities (data not shown).

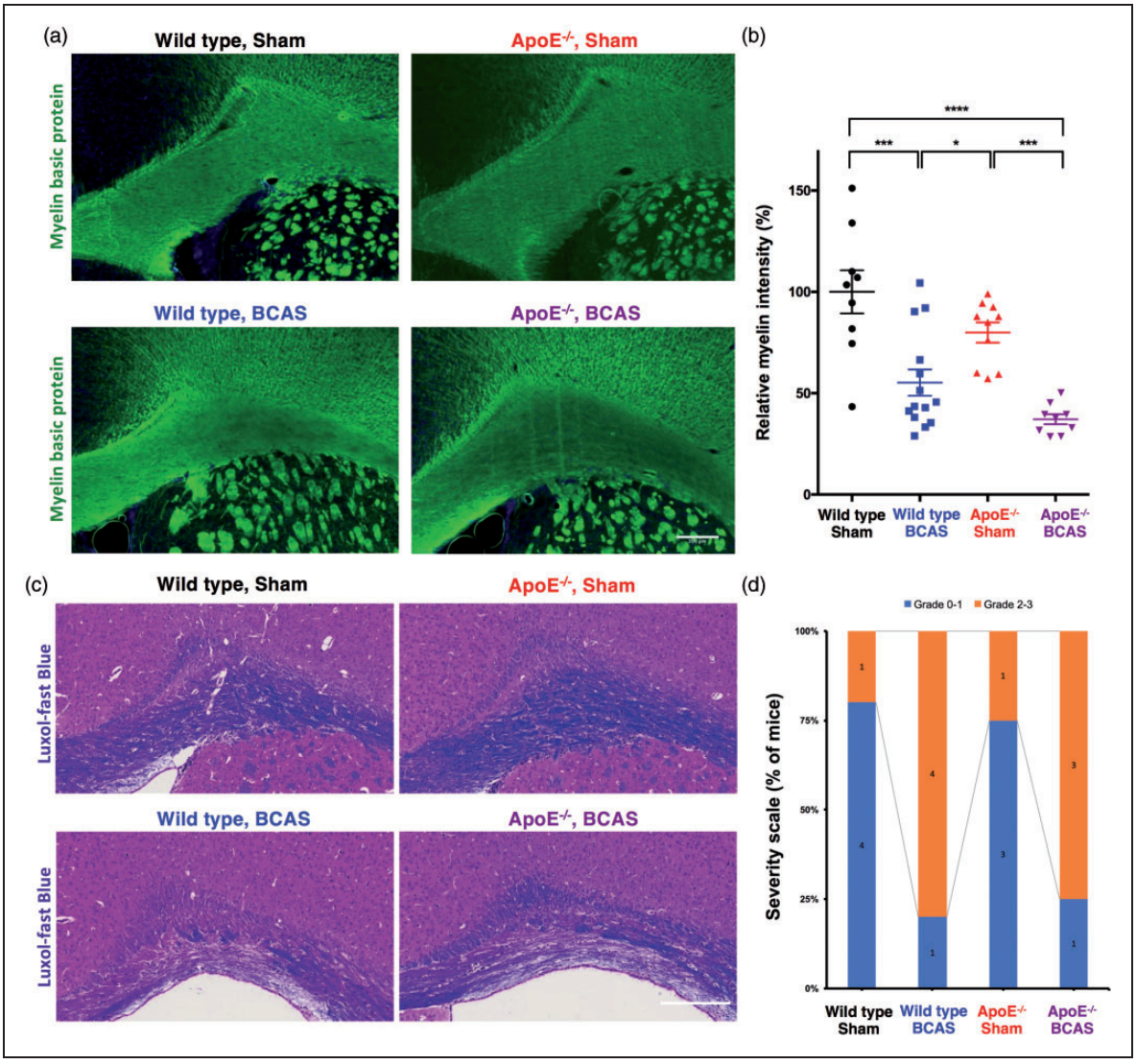

Figure 2. White matter damages. (a) Representative images of white matter staining (immunofluorescence staining of myelin basic protein; scale bar, 200 μm). (b) Quantification of relative myelin density (mean ± s.e.m.; 9 wild-type sham, 14 wild-type BCAS, 10 ApoE$^{-/-}$ sham, and 9 ApoE$^{-/-}$ BCAS mice; significance for multiple comparisons: *$P < 0.05$; **$P < 0.01$; ***$P < 0.001$; ****$P < 0.0001$). Data are expressed as a percentage of the myelin density in wild-type sham-operated mice. (c) A representative image of white matter damage defined by LFB staining (scale bar, 200 μm). (d) Severity score of white matter damage from LFB staining. (Data are presented as number of mice; five wild-type sham, five wild-type BCAS, four ApoE$^{-/-}$ sham, and four ApoE$^{-/-}$ BCAS mice).

Wild-type mice did not show any microinfarction lesions after BCAS surgery, as previous reported.[4] In contrast, three of the four ApoE$^{-/-}$ mice had multiple microinfarctions and hippocampal neuronal loss six weeks after the BCAS operation. Figure 3 depicts the hippocampal neuronal loss and multiple microinfarction lesions, as defined by H&E staining and IHC for CD68, in the cortical and subcortical areas of ApoE$^{-/-}$ mice that had undergone BCAS.

Marked astroglial activation was observed in widespread brain regions in the ApoE$^{-/-}$-BCAS group (Figure 4(a)). In the cerebral cortex, ApoE$^{-/-}$-BCAS mice showed prominent astroglial activation, with a 289.2% increase compared to wild-type sham-operated mice (Figure 4(b)). A two-way ANOVA followed by Tukey's multiple comparison test revealed a significant effect for the BCAS operation ($F(1,46) = 15.12$, $P = 0.0003$) and genotype ($F(1,46) = 48.50$, $P < 0.0001$), and a significant interaction between genotype and BCAS operation ($F(1,46) = 16.76$, $P < 0.0002$). Hippocampi from BCAS-operated ApoE$^{-/-}$ mice had astroglial activation, with a 241% increase in astrogliosis compared to wild-type sham-operated mice (Figure 4(b)). A two-way ANOVA followed by Tukey's multiple comparison test revealed significant effects for the BCAS operation ($F(1,46) = 8.699$, $P = 0.005$) and genotype ($F(1,46) = 30.07$, $P < 0.0001$), but no significant interaction between genotype and BCAS operation ($F(1,46) = 2.914$, $P = 0.0946$). The white matter of BCAS-operated wild-type and ApoE$^{-/-}$ mice showed a

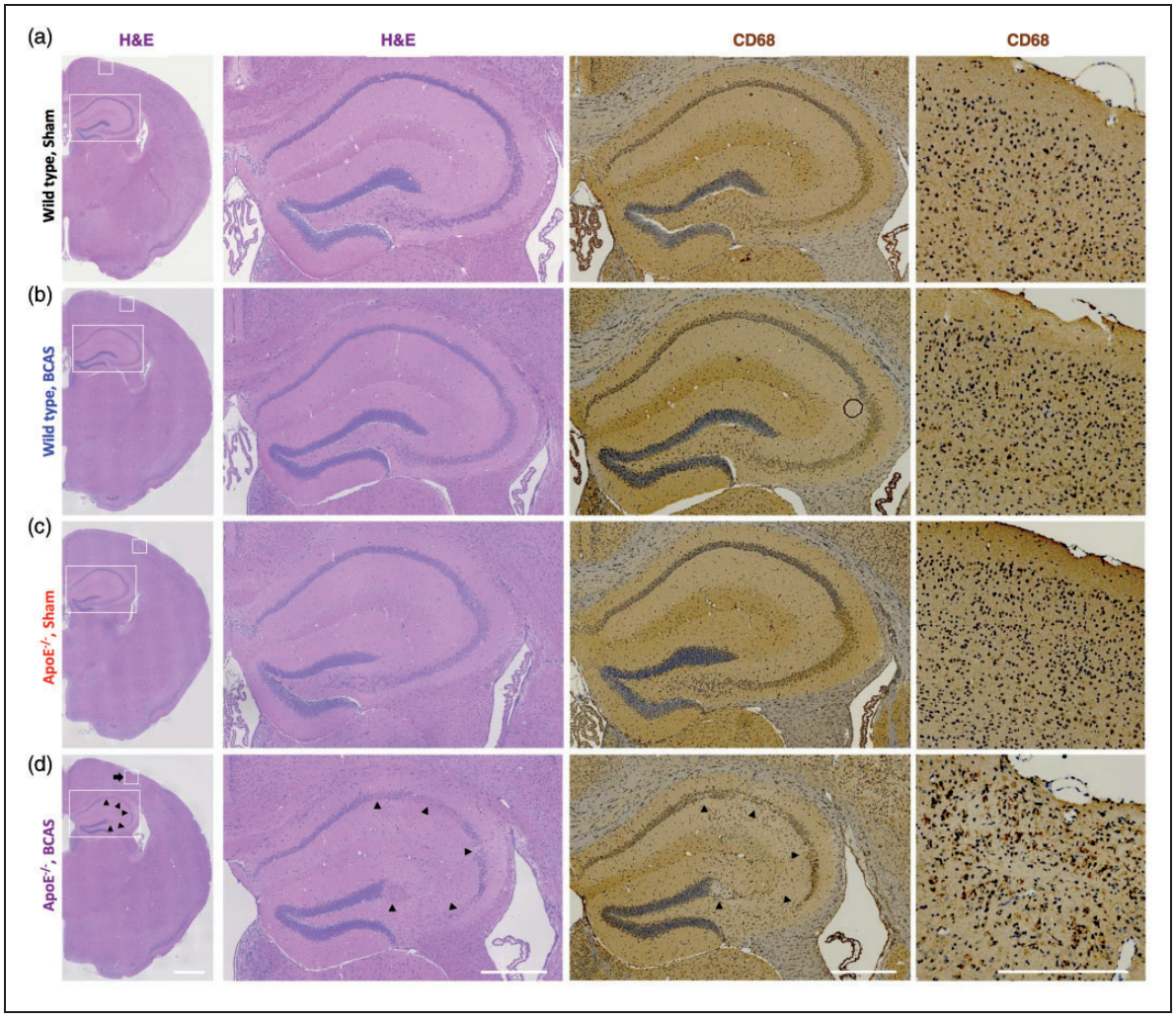

Figure 3. Hippocampal neuronal loss and multiple microinfarctions. (a) Wild-type sham, (b) wild-type BCAS, (c) ApoE$^{-/-}$ sham, and (d) ApoE$^{-/-}$ BCAS mice. Hippocampal neuronal loss (arrowheads) and ischemic stroke (arrow) was seen only in ApoE$^{-/-}$ BCAS mice (three of four ApoE$^{-/-}$ BCAS mice). Scale bars, 200 μm.

180.9% and 203.7% increase, respectively, in astroglial activation compared to wild-type sham-operated mice (Figure 4(b)). A two-way ANOVA followed by a Tukey's multiple comparison test revealed significant effects for the BCAS operation ($F(1,46) = 32.85$, $P < 0.0001$) and genotype ($F(1,46) = 5.24$, $P = 0.0267$), but no significant interaction between genotype and BCAS operation ($F(1,46) = 0.2765$, $P = 0.6015$). Taken together with the MBP immunostaining results, these findings indicate that chronic cerebral hypoperfusion had greater influence on myelin loss and astroglial activation in the white matter than ApoE deficiency.

Since ageing is an important risk factor for vascular dementia, we investigated whether similar results were

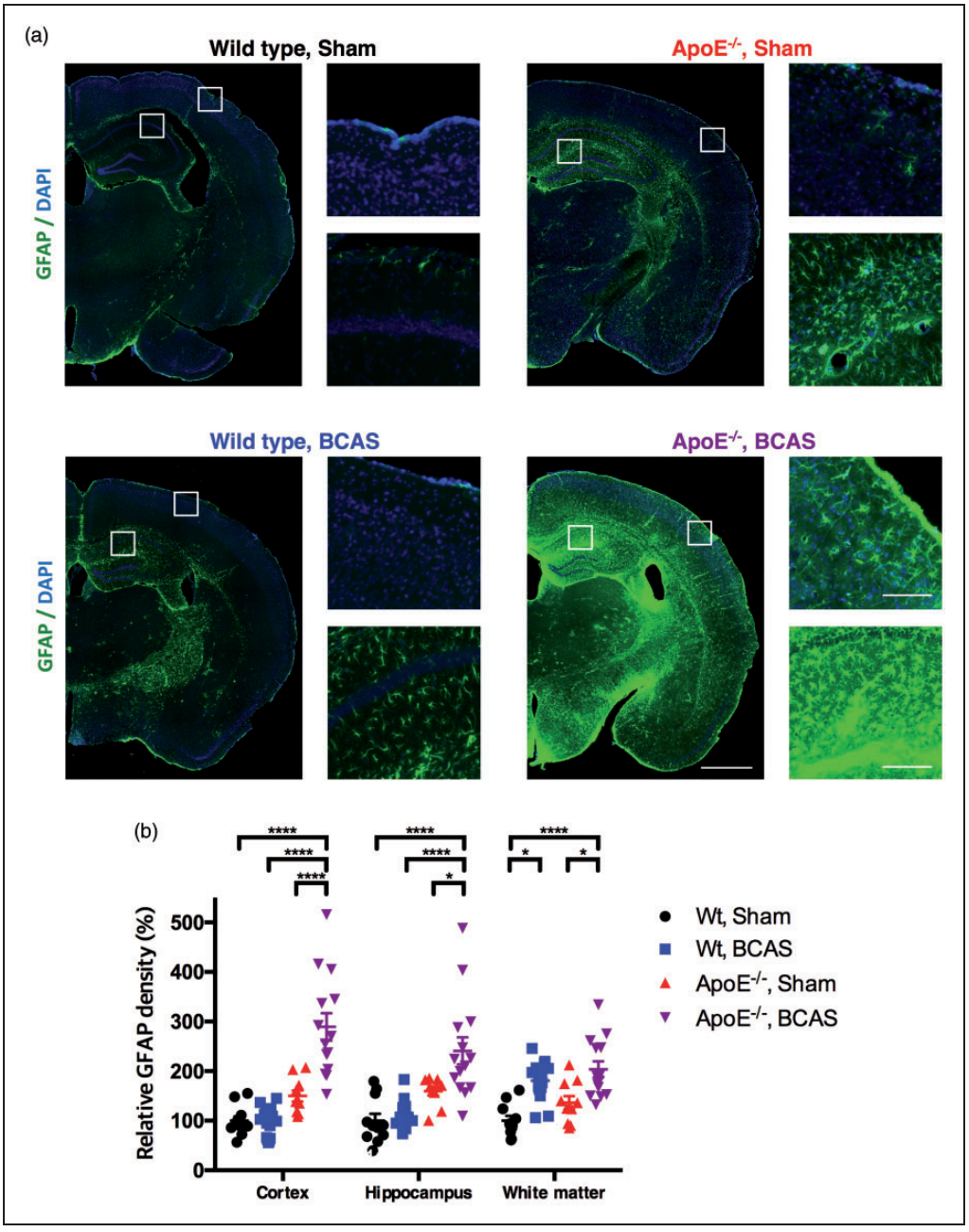

Figure 4. Extensive astrogliosis. (a) Representative images of coronal brain sections immunostained for GFAP (wild-type sham, left panel of the upper row; wild-type BCAS, left panel of the lower row; $ApoE^{-/-}$ sham, right panel of the upper row; $ApoE^{-/-}$ BCAS, right panel of the lower row). Scale bar, 1000 μm for low magnitude images; 100 μm for high magnitude images. (b) Data are expressed as a percentage of the glial activation observed in the wild-type sham group. Mean ± s.e.m.; 11 wild-type sham, 15 wild-type BCAS, 10 $ApoE^{-/-}$ sham, and 14 $ApoE^{-/-}$ BCAS mice; significance for multiple comparisons: $^{*}P < 0.05$; $^{**}P < 0.01$; $^{***}P < 0.001$; $^{****}P < 0.0001$.

seen in aged mice. The results were similar to those found in young mice, with the exception that there was more extensive ischemic stroke in ApoE$^{-/-}$ BCAS mice (Supplementary Figures 1 and 2).

Alterations in cerebral microcirculation

Immunostaining indicated that there were 22.95% and 23.68% reductions in the area of the cerebral cortex positive for the endothelial marker CD31 in ApoE$^{-/-}$ sham and ApoE$^{-/-}$ BCAS mice, respectively (Figure 5(a)). A two-way ANOVA followed by a Tukey's multiple comparison test revealed a significant effect of genotype ($F(1,37) = 14.19$, $P = 0.0006$), but no significant effect of operation and no interaction between genotype and BCAS operation (Figure 5(b)).

To examine whether the observed microvasculature reductions reflected impaired microcirculation in vivo, we used in vivo multi-photon microscopy following an injection of a fluorescent dextran to obtain a cortical angiogram. Analysis of the reconstructed images revealed a 14.5% decrease in perfused capillary length in ApoE$^{-/-}$ sham-operated mice and a 14.6% reduction in perfused capillary length in ApoE$^{-/-}$ BCAS mice (Figure 5(c) and (d)). A two-way ANOVA followed by a Tukey's multiple comparison test revealed a significant effect of genotype ($F(1,13) = 6.918$, $P = 0.0208$), but no significant effect of operation and no interaction between genotype and BCAS operation. These results suggest that ApoE$^{-/-}$ alone was sufficient to reduce cerebral microcirculation, and that there was no synergistic effect between ApoE$^{-/-}$ genotype and BCAS operation.

Immunostaining for endogenous immunoglobulin G (IgG) revealed significantly increased IgG intensity in the cerebral cortex, hippocampus, and white matter of ApoE$^{-/-}$ BCAS mice compared to wild-type sham, wild-type BCAS, and ApoE$^{-/-}$ sham mice (Figure 6). A two-way ANOVA followed by a Tukey's multiple comparison test revealed an interaction between genotype and BCAS operation in the cortex and hippocampus, but not in the white matter. These data indicate that breakdown of the BBB in the cortex and hippocampus is further worsened in ApoE$^{-/-}$ BCAS mice compared to both ApoE$^{-/-}$ and BCAS-operated mice.

Impaired locomotion and memory

Total distance travelled in the open field test was significantly decreased in ApoE$^{-/-}$BCAS mice (Figure 7(a)). A two-way ANOVA followed by Tukey's multiple comparison test a revealed significant effect of BCAS operation [$F(1,23) = 8.517$, $P = 0.0077$], no significant effect of genotype, and no interaction between genotype and BCAS operation. These results revealed a substantial locomotor deficit in ApoE$^{-/-}$BCAS-operated mice.

The Y-maze test revealed a significant decrease in spontaneous alternation behaviour in wild-type BCAS and ApoE$^{-/-}$ BCAS mice compared to sham-operated wild-type or ApoE$^{-/-}$ mice (Figure 7(b)). A two-way ANOVA followed by a Tukey's multiple comparison test revealed a significant effect of BCAS operation ($F(1,23) = 38.78$, $P < 0.0001$), but no significant effect of genotype and no interaction between genotype and BCAS operation.

In the novel object recognition test, all groups, except for ApoE$^{-/-}$BCAS, displayed normal recognition memory for a preconditioned (familiar) object, which was presented 2 h before the test. However, there was no difference in the time ApoE$^{-/-}$BCAS mice spent with the preconditioned object than with the novel object, suggesting impaired recognition memory (Figure 7(c)). The exploration ratio (normalized ratio of time spent with the novel object minus the time spent with the preconditioned object, divided by the sum of the time spent with the novel and preconditioned objects) was significantly decreased in ApoE$^{-/-}$ BCAS mice when compared to wild-type and ApoE$^{-/-}$ sham-operated mice (Figure 7(d)). A two-way ANOVA followed by a Tukey's multiple comparison test revealed significant effects of genotype ($F(1,23) = 4.475$, $P = 0.0423$) and BCAS operation ($F(1,23) = 4.65$, $P < 0.0387$), and an interaction between genotype and BCAS operation ($F(1,23) = 5.318$, $P < 0.0277$).

Based on our behavioural results, we found that BCAS-operated ApoE$^{-/-}$ mice displayed impairments in locomotion, spatial working memory, and recognition memory, revealing that this mouse model effectively mimicked the neurological deficits associated with human SVaD. No differences were found among the groups in weight or food consumption (Supplementary Figure 3).

Discussion

In the current study, we developed a mouse model of SVaD using BCAS-operated ApoE$^{-/-}$ mice. These mice showed white matter damage, multiple microinfarctions, degeneration of cerebral microcirculation, and neurological deficits, which mimicked core clinicopathological features of human SVaD. In particular, multiple microinfarctions, decreased locomotor activity, and impaired recognition memory was observed in the proposed model but not in other groups.

Degeneration of cerebral microcirculation, such as microvasculature reduction and BBB breakdown, is a crucial pathological feature of SVaD.[6] Patients with SVaD exhibit reductions in capillary density and increased non-functional capillaries, known as

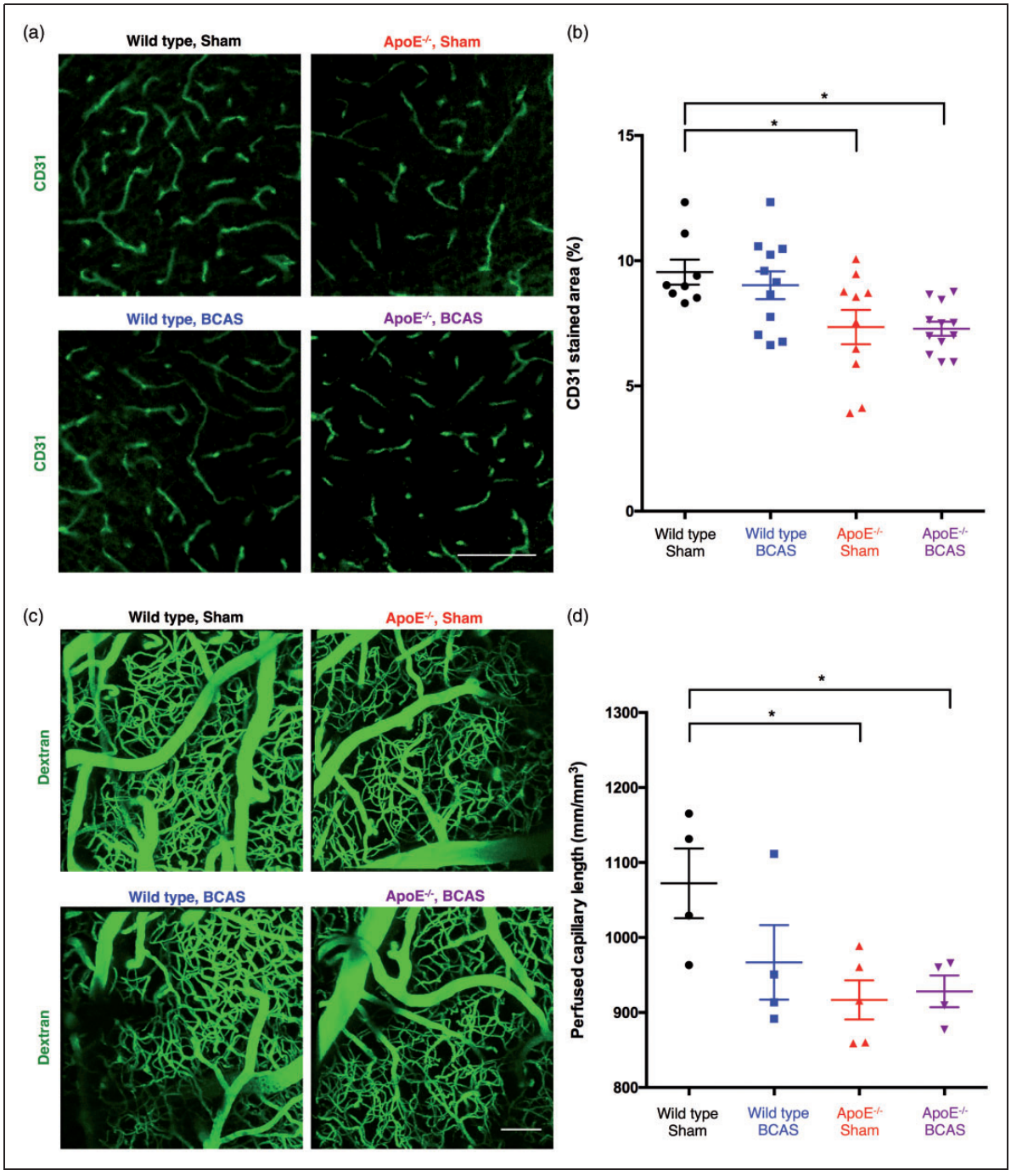

Figure 5. Reductions in cerebral microcirculation. (a) Representative images of CD31-stained microvessels. Scale bar, 500 μm. (b) Quantification of CD31-positive microvessels in the cortex. Mean ± s.e.m.; 8 wild-type sham, 11 wild-type BCAS, 10 ApoE$^{-/-}$ sham, and 12 ApoE$^{-/-}$ BCAS mice; significance for multiple comparisons: *$P < 0.05$. (c) Decreased perfused capillary length in ApoE$^{-/-}$ mice. Perfusion of cortical microvessels revealed by in vivo multi-photon microscopy of FITC-conjugated dextran. Scale bar, 100 μm. (d) Quantification of perfused capillary length. Mean ± s.e.m.; four wild-type sham, four wild-type BCAS, five ApoE$^{-/-}$ sham, and four ApoE$^{-/-}$ BCAS mice; significance for multiple comparisons: *$P < 0.05$.

"string-vessels," both in normal-appearing and damaged white matter.[26] In addition to microvasculature reductions, several lines of evidence indicate that the BBB is disrupted over the course of SVaD.[11–14,27–31] In our study, decreases in microvasculature density, revealed by in vivo and ex vivo analyses, were observed only in ApoE$^{-/-}$ mice, regardless of BCAS operation. These findings are consistent with those of a previous

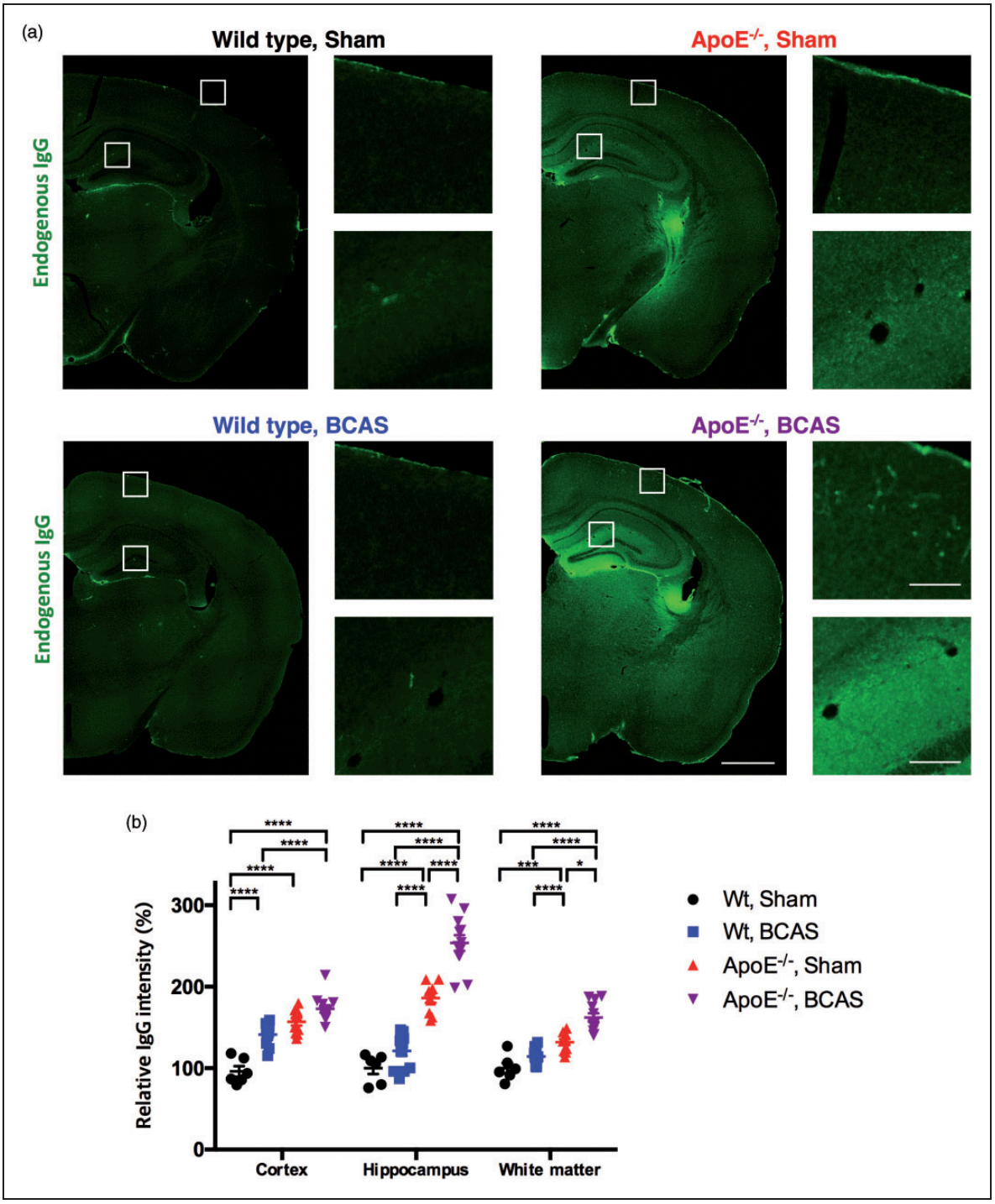

Figure 6. BBB breakdown revealed by endogenous IgG staining. (a) Marked leakage of endogenous IgG in the hippocampus of ApoE$^{-/-}$ sham and ApoE$^{-/-}$ BCAS mice (left); Scale bar, 1000 μm for low magnitude images; 100 μm for high magnitude images. (b) Quantification of endogenous IgG leakage. Data are expressed as percentages of the IgG fluorescence signal observed in the wild-type sham group. Mean ± s.e.m.; 6 wild-type sham, 12 wild-type BCAS, 10 ApoE$^{-/-}$ sham, and 12 ApoE$^{-/-}$ BCAS mice; significance for multiple comparisons: *$P < 0.05$; **$P < 0.01$; ***$P < 0.001$; ****$P < 0.0001$.

study indicating that capillary length is reduced in ApoE$^{-/-}$ mice.[20] In contrast, BCAS-operated ApoE$^{-/-}$ mice had increased endogenous IgG due to BBB breakdown in cortical and hippocampal areas when compared to BCAS-operated wild-type mice. This suggests that ApoE deficiency worsens BBB breakdown after chronic cerebral hypoperfusion. Taken together, our histological examinations revealed that

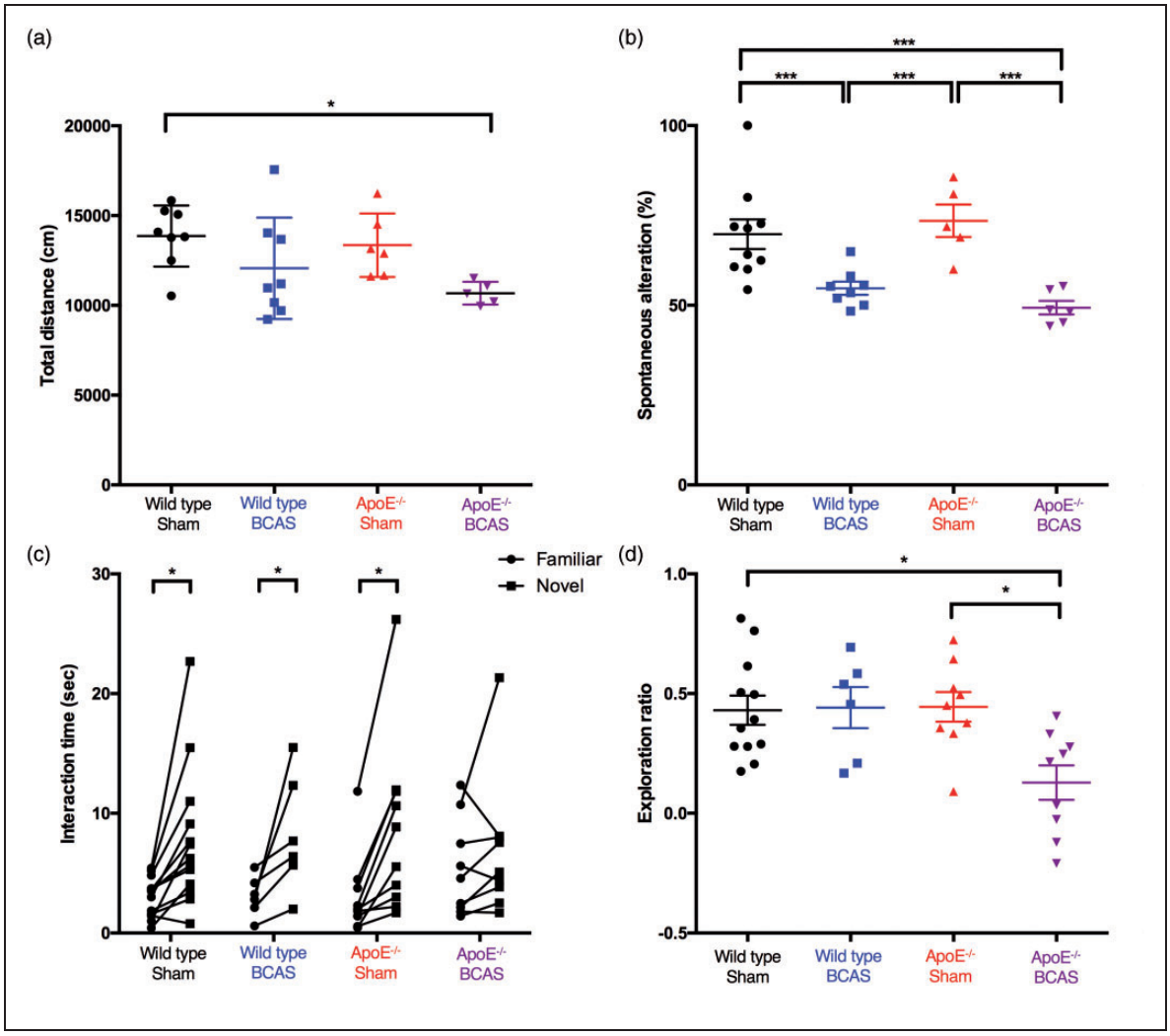

Figure 7. Behavioural results. (a) Locomotor activity in an open field test. Total distance travelled was decreased only in ApoE$^{-/-}$ BCAS mice. Eight wild-type sham, eight wild-type BCAS, five ApoE$^{-/-}$ sham, and six ApoE$^{-/-}$-BCAS mice. (b) Spatial working memory in the Y-maze test. The percentage of spontaneous alternation behaviour significantly decreased in wide-type BCAS and ApoE$^{-/-}$ BCAS mice compared with sham-operated mice. Eight wild-type sham, eight wild-type BCAS, five ApoE$^{-/-}$ sham, and six ApoE$^{-/-}$ BCAS mice. Significance for multiple comparisons (a and b): *$P < 0.05$; **$P < 0.01$; ***$P < 0.001$; ****$P < 0.0001$. (c and d) Novel object recognition test. (c) Time spent exploring novel and familiar objects (Student's *t*-test, *$P < 0.05$ compared to time spent with the familiar object). (d) Exploration ratio (12 wild-type sham, 6 wild-type BCAS, 9 ApoE$^{-/-}$ sham, and 9 ApoE$^{-/-}$ BCAS mice; two-way ANOVA followed by Tukey's post hoc analysis, *$P < 0.05$).

our mouse model more precisely mimics human SVaD pathology in terms of the degeneration of cerebral microcirculation than any of the currently available animal models of SVaD.

Another possible explanation for the worsened outcome observed in ApoE$^{-/-}$ mice after BCAS surgery might be related to severe cerebral hypoperfusion. Chronic cerebral hypoperfusion can also cause disruption of the BBB.[32] Several studies have shown the molecular cascades which are initiated following induction of hypoxia inducible factor-1α (HIF1A) by hypoperfusion. HIF1A activates matrix metalloproteinases and inflammatory cytokines that lead to degradation of tight junction proteins and neuroinflammatory responses.[32–35] As shown in Figure 2, CBF values in wild-type mice 2 h after BCAS surgery dropped from the preoperative baseline measures, began to recover one day post-surgery, and reached 75.4% of the baseline values by seven days after surgery. In contrast, CBF values dropped sharply in ApoE$^{-/-}$ mice and failed to recover. Together, these results led us to speculate that BCAS and ApoE deficiency may act synergistically to reduce CBF. The histopathological and behavioural features were investigated up to six weeks after surgery, while CBF was studied for only one week. However, several studies have reported that there is no

significant difference in CBF between one week and one month after BCAS operation. Therefore, we assumed that CBF changes would show a similar tendency in our experiments.

During the clinical course of SVaD, neuropsychological tests have revealed impairments in working memory, attention, execution, set-shifting performances, and verbal fluency. Such disruptions are attributed to damaged fronto-subcortical circuits.[1] Along with cognitive impairments, neurological deficits, including gait disturbances, are common in patients with SVaD.[36,37] In the current study, BCAS-operated ApoE$^{-/-}$ mice exhibited impairments in locomotion (gait), working memory, and object-recognition memory, demonstrating that our mouse model reflected not only pathological features of human SVaD, but also cognitive and behavioural aspects of the disease. Since a reduction in locomotor activity can negatively affect mouse activity, our interpretations of the other behavioural tasks may have been confounded.

Some points should be carefully considered when interpreting our statistical results. Sample sizes were not calculated before the experiments and the group sizes for the different experiments were not the same. However, a post hoc power analysis was conducted and showed that the statistical power exceeded 80.0% for most of the tests (the exceptions were CD31 staining and capillary length). The numbers of animals in the different groups in this study were thus sufficient to detect statistically significant differences, except for those in CD31 staining and capillary length.

In conclusion, by combining animal models of chronic cerebral hypoperfusion and atherosclerosis, we developed a mouse model of SVaD which showed cognitive decline, impaired locomotion, white matter degeneration, and cerebral microcirculation deficits. These pathological, cognitive, and behavioural features are comparable to those observed in patients with SVaD. Therefore, our model might prove useful in studying the pathophysiology and potential therapeutic interventions for SVaD.

Funding

The author(s) disclosed receipt of the following financial support for the research, authorship, and/or publication of this article: This work was supported by the R&D Program of Daegu-Gyeongbuk Medical Innovation Foundation [grant number HI13C1015] and by the Brain Research Program through the National Research Foundation of Korea (NRF) funded by the Ministry of Science and ICT [grant number 2016M3C7A1913844].

Declaration of conflicting interests

The author(s) declared no potential conflicts of interest with respect to the research, authorship, and/or publication of this article.

Authors' contributions

E-SL, as the first author, contributed to all aspects of data analysis and interpretation of the data, and drafting of the manuscript. YJ, as the corresponding author, contributed to design of the study, interpretation of the data. J-HY, JC, FRA, and T-KL contributed to data correction, data analysis and critical revision of the manuscripts.

Supplementary material

Supplementary material for this paper can be found at the journal website: http://journals.sagepub.com/home/jcb

References

1. Choi SH, Kim S, Han SH, et al. Neurologic signs in relation to cognitive function in subcortical ischemic vascular dementia: a CREDOS (Clinical Research Center for Dementia of South Korea) study. *Neurol Sci* 2012; 33: 839–846.
2. Gorelick PB, Scuteri A, Black SE, et al. Vascular contributions to cognitive impairment and dementia: a statement for healthcare professionals from the American Heart Association/American Stroke Association. *Stroke* 2011; 42: 2672–2713.
3. Lee JH, Kim SH, Kim GH, et al. Identification of pure subcortical vascular dementia using 11C-Pittsburgh compound B. *Neurology* 2011; 77: 18–25.
4. Tomimoto H. Subcortical vascular dementia. *Neurosci Res* 2011; 71: 193–199.
5. Raz L, Knoefel J and Bhaskar K. The neuropathology and cerebrovascular mechanisms of dementia. *J Cereb Blood Flow Metab* 2016; 36: 172–186.
6. Iadecola C. The pathobiology of vascular dementia. *Neuron* 2013; 80: 844–866.
7. Seo SW, Ahn J, Yoon U, et al. Cortical thinning in vascular mild cognitive impairment and vascular dementia of subcortical type. *J Neuroimaging* 2010; 20: 37–45.
8. Farkas E, De Jong GI, de Vos RA, et al. Pathological features of cerebral cortical capillaries are doubled in Alzheimer's disease and Parkinson's disease. *Acta Neuropathol* 2000; 100: 395–402.
9. Schreiber S, Bueche CZ, Garz C, et al. Blood brain barrier breakdown as the starting point of cerebral small vessel disease? New insights from a rat model. *Exp Transl Stroke Med* 2013; 5: 4.
10. Wardlaw JM, Sandercock PA, Dennis MS, et al. Is breakdown of the blood-brain barrier responsible for lacunar stroke, leukoaraiosis, and dementia? *Stroke* 2003; 34: 806–812.
11. Yang Y and Rosenberg GA. Blood-brain barrier breakdown in acute and chronic cerebrovascular disease. *Stroke* 2011; 42: 3323–3328.
12. Hanyu H, Asano T, Tanaka Y, et al. Increased blood-brain barrier permeability in white matter lesions of Binswanger's disease evaluated by contrast-enhanced MRI. *Dement Geriatr Cogn Disord* 2002; 14: 1–6.
13. Taheri S, Gasparovic C, Huisa BN, et al. Blood-brain barrier permeability abnormalities in vascular cognitive impairment. *Stroke* 2011; 42: 2158–2163.

14. Topakian R, Barrick TR, Howe FA, et al. Blood-brain barrier permeability is increased in normal-appearing white matter in patients with lacunar stroke and leucoaraiosis. *J Neurol Neurosurg Psychiatry* 2010; 81: 192–197.
15. Ihara M and Tomimoto H. Lessons from a mouse model characterizing features of vascular cognitive impairment with white matter changes. *J Aging Res* 2011; 2011: 978761.
16. Shibata M, Ohtani R, Ihara M, et al. White matter lesions and glial activation in a novel mouse model of chronic cerebral hypoperfusion. *Stroke* 2004; 35: 2598–2603.
17. Nishio K, Ihara M, Yamasaki N, et al. A mouse model characterizing features of vascular dementia with hippocampal atrophy. *Stroke* 2010; 41: 1278–1284.
18. Mahley RW. Apolipoprotein E: cholesterol transport protein with expanding role in cell biology. *Science* 1988; 240: 622–630.
19. Bink DI, Ritz K, Aronica E, et al. Mouse models to study the effect of cardiovascular risk factors on brain structure and cognition. *J Cereb Blood Flow Metab* 2013; 33: 1666–1684.
20. Bell RD, Winkler EA, Singh I, et al. Apolipoprotein E controls cerebrovascular integrity via cyclophilin A. *Nature* 2012; 485: 512–516.
21. Okamoto Y, Yamamoto T, Kalaria RN, et al. Cerebral hypoperfusion accelerates cerebral amyloid angiopathy and promotes cortical microinfarcts. *Acta Neuropathol* 2012; 123: 381–394.
22. Hattori Y, Enmi JI, Kitamura A, et al. A novel mouse model of subcortical infarcts with dementia. *J Neurosci* 2015; 35: 3915–3928.
23. Yoon HJ, Lee ES, Kang M, et al. In vivo multi-photon luminescence imaging of cerebral vasculature and blood-brain barrier integrity using gold nanoparticles. *J Mat Chem B* 2015; 3: 2935–2938.
24. Bell RD, Winkler EA, Sagare AP, et al. Pericytes control key neurovascular functions and neuronal phenotype in the adult brain and during brain aging. *Neuron* 2010; 68: 409–427.
25. Washida K, Ihara M, Nishio K, et al. Nonhypotensive dose of telmisartan attenuates cognitive impairment partially due to peroxisome proliferator-activated receptor-gamma activation in mice with chronic cerebral hypoperfusion. *Stroke* 2010; 41: 1798–1806.
26. Cohen J. *Statistical power analysis for the behavioral sciences*, 2nd ed. Hinsdale, NJ: Lawrence Erlbaum Associates, 1988.
27. Brown WR, Moody DM, Thore CR, et al. Vascular dementia in leukoaraiosis may be a consequence of capillary loss not only in the lesions, but in normal-appearing white matter and cortex as well. *J Neurol Sci* 2007; 257: 62–66.
28. Tomimoto H, Akiguchi I, Suenaga T, et al. Alterations of the blood-brain barrier and glial cells in white-matter lesions in cerebrovascular and Alzheimer's disease patients. *Stroke* 1996; 27: 2069–2074.
29. Simpson JE, Fernando MS, Clark L, et al. White matter lesions in an unselected cohort of the elderly: astrocytic, microglial and oligodendrocyte precursor cell responses. *Neuropathol Appl Neurobiol* 2007; 33: 410–419.
30. Alafuzoff I, Adolfsson R, Grundke-Iqbal I, et al. Perivascular deposits of serum proteins in cerebral cortex in vascular dementia. *Acta Neuropathol* 1985; 66: 292–298.
31. Akiguchi I, Tomimoto H, Suenaga T, et al. Blood-brain barrier dysfunction in Binswanger's disease; an immunohistochemical study. *Acta Neuropathol* 1998; 95: 78–84.
32. Candelario-Jalil E, Thompson J, Taheri S, et al. Matrix metalloproteinases are associated with increased blood-brain barrier opening in vascular cognitive impairment. *Stroke* 2011; 42: 1345–1350.
33. Ueno M, Tomimoto H, Akiguchi I, et al. Blood-brain barrier disruption in white matter lesions in a rat model of chronic cerebral hypoperfusion. *J Cereb Blood Flow Metab* 2002; 22: 97–104.
34. Seo JH, Miyamoto N, Hayakawa K, et al. Oligodendrocyte precursors induce early blood-brain barrier opening after white matter injury. *J Clin Invest* 2013; 123: 782–786.
35. Armao D, Kornfeld M, Estrada EY, et al. Neutral proteases and disruption of the blood-brain barrier in rat. *Brain Res* 1997; 767: 259–264.
36. Braun H, Bueche CZ, Garz C, et al. Stases are associated with blood-brain barrier damage and a restricted activation of coagulation in SHRSP. *J Neurol Sci* 2012; 322: 71–76.
37. Roh JH and Lee JH. Recent updates on subcortical ischemic vascular dementia. *J Stroke* 2014; 16: 18–26.